EUROPEAN ORGANIZATION FOR NUCLEAR RESEARCH
CERN – ACCELERATORS AND TECHNOLOGY SECTOR

Multipactor Mitigation in Coaxial Lines by Means of Permanent Magnets

D. Gonzalez-Iglesias, A. M. Perez, S. Anza, J. Vague, B. Gimeno, Member, IEEE, V. E. Boria, Senior Member, IEEE, D. Raboso, C. Vicente, J. Gil, F. Caspers, Senior Member, IEEE, L. Conde

Abstract

The main aim of this paper is the analysis of the feasibility of employing permanent magnets for the multipactor mitigation in a coaxial waveguide. First, the study of a coaxial line immersed in a uniform axial magnetic field shows that multipactor can be suppressed at any RF frequency if the external magnetic field is strong enough. Both theoretical simulations and experimental tests validate this statement. Next, multipactor breakdown of a coaxial line immersed in a hollow cylindrical permanent magnet is analyzed. Numerical simulations show that multipactor can be suppressed in a certain RF frequency range. The performed experimental test campaign demonstrates the capability of the magnet to avoid the multipactor electron multiplication process.

Published in: IEEE TRANSACTIONS ON ELECTRON DEVICES, VOL. 61, NO. 12, DECEMBER 2014

Multipactor Mitigation in Coaxial Lines by Means of Permanent Magnets

D. González-Iglesias, A. M. Pérez, S. Anza, J. Vague, B. Gimeno, *Member, IEEE*, V. E. Boria, *Senior Member, IEEE*, D. Raboso, C. Vicente, J. Gil, F. Caspers, *Senior Member, IEEE*, L. Conde

***Abstract*—The main aim of this paper is the analysis of the feasibility of employing permanent magnets for the multipactor mitigation in a coaxial waveguide. First, the study of a coaxial line immersed in a uniform axial magnetic field shows that multipactor can be suppressed at any RF frequency if the external magnetic field is strong enough. Both theoretical simulations and experimental tests validate this statement. Next, multipactor breakdown of a coaxial line immersed in a hollow cylindrical permanent magnet is analyzed. Numerical simulations show that multipactor can be suppressed in a certain RF frequency range. The performed experimental test campaign demonstrates the capability of the magnet to avoid the multipactor electron multiplication process.**

***Index Terms*—Multipactor effect, RF breakdown, permanent magnet, DC magnetic field, coaxial waveguide, multipactor mitigation.**

I. Introduction

The multipactor effect is a resonant vacuum electron discharge that appears in components operating with RF high-power electromagnetic fields [1]. This phenomenon is present in many different environments such as RF satellite payloads, particle accelerators, klystrons or cyclotrons. When certain conditions are satisfied, the free electrons synchronize with the RF electric field, and impact against the metallic walls releasing secondary electrons. Thus, the increase of the electron population in the device leads to an electrical discharge that degrades the component performance and can physically damage the structure.

This RF breakdown effect has been the subject of a number of studies addressed to designing multipactor free RF components. Several techniques are applicable for avoiding this undesirable effect, such as chemical polishing, groove insertions in the metal surface, surface coatings or changes in the gap dimensions. However, surface treatments degrade in time, surface grooves impair the RF performance and geometrical modifications are unpractical in most microwave components. Recently, some authors proposed the use of DC magnetic fields for the partial or total discharge mitigation. Sometimes, the direction of the applied magnetic field is oriented along the transverse plane for a coaxial geometry [2], whilst an axial magnetic field is inserted for multipactor suppression in rectangular waveguides [3]-[7].

The multipactor effect in a coaxial line under the presence of a uniform axial static magnetic field was investigated in a previous paper [8]. These results evidence that RF power thresholds (the lowest RF power value at which the multipactor discharge appears) are strongly influenced by the magnitude of the magnetic field. These results were obtained for a fixed RF frequency. In this paper, we extend this previous study by analyzing the effect of the RF frequency signal, as well as the magnetic field strength. As we shall see, the total suppression of multipactor breakdown can be obtained regardless of the RF signal frequency for magnetic field strengths over a onset. In addition, we discuss about the feasibility of multipactor suppression by means of the realistic non-uniform magnetic field pattern of neodymium permanent magnets.

This paper is structured as follows. Section II-A describes the physical model used in our simulation code to perform the numerical calculations of multipactor breakdown. In section II-B, we derive analytical expressions for the magnetic field strength produced by a magnetized hollow cylinder. Section III-A analyzes the effect of a uniform DC magnetic field on the multipactor power threshold showing both theoretical simulations and experimental results. Next, in section III-B, the implementation of a non-uniform magnetic field along the coaxial line by means of a hollow neodymium magnet, is investigated. According to the required specifications, a neodymium magnet has been designed and manufactured to carry out experimental tests in order to validate the theoretical results. Finally, the conclusions are drawn in Section IV.

II. Theory

A. Multipactor algorithm

In this paper, we use a Monte-Carlo code to perform the simulations of multipactor in coaxial transmission lines using the traditional single effective electron model [10], [11]. This technique is based on the 3D tracking of a set of effective electrons governed by the electromagnetic field. The trajectory of the effective electron is found numerically solving its equation of motion (expressed in Cartesian co-ordinates) by means of the Velocity-Verlet algorithm [12]. Each effective electron describes a particular electronic population which evolves in time by colliding with the coaxial metallic walls of the waveguide. The secondary electron yield (SEY) function (δ) is computed after each impact as a function of the impact kinetic energy and impinging angle by means of the SEY

D. González-Iglesias and B. Gimeno is with Depto. Física Aplicada-ICMUV, Universidad de Valencia, Spain

A. M. Pérez, J. Vague and V. E. Boria are with Depto. Comunicaciones-iTEAM, Universidad Politécnica de Valencia, Spain

S. Anza, C. Vicente and J. Gil are with AURORASAT, Valencia, Spain

D. Raboso is with European Space Agency, ESA/ESTEC, The Netherlands

F. Caspers is with CERN, Geneva, Switzerland

L. Conde is with Depto. Física Aplicada, E.T.S.I. Aeronáuticos, Universidad Politécnica de Madrid, Spain

model formulated in [13], [14]. After that, the colliding electron is re-emitted from the impact place with random initial velocity given by a Maxwellian distribution with a mean average energy of 3 eV. The velocity launching angle is given by the cosine law [15].

The total driving electromagnetic field experienced on each effective electron is the sum of three contributions: the excited RF fields, the electric field due to the Coulombian repulsion among electrons, and an applied external DC magnetic field. The excited RF fields are those related to the fundamental mode of the coaxial guide at frequency f. The electric field caused by the electron cloud is modelled by means of a single electron sheet, following the same procedure proposed in [16]. Two different kinds of external DC magnetic field will be considered in the present work. First, in section III-A, a uniform magnetic field oriented along the axial direction of the coaxial line. Second, in Section III-B, the coaxial sample is immersed into a hollow cylindrical permanent magnet. In this case the non-uniform magnetic field has radial and axial components.

The effective electron dynamics is governed by the non-relativistic Lorentz force expression leading to [17],

$$\frac{dv_r}{dt} = \frac{d^2r}{dt^2} - r\left(\frac{d\phi}{dt}\right)^2 = -\frac{e}{m}\Bigg[E_{RF}(\vec{r},t) + E_{sc}(\vec{r},t) - \tag{1}$$

$$+ B_{RF}(\vec{r},t)\, v_z + B_{ext,z}(\vec{r})\, v_\phi\Bigg]$$

$$\frac{dv_\phi}{dt} = r\frac{d^2\phi}{dt^2} + 2\frac{dr}{dt}\frac{d\phi}{dt} = -\frac{e}{m}\left[-B_{ext,z}(\vec{r})\, v_r + B_{ext,r}(\vec{r})\, v_z\right] \tag{2}$$

$$\frac{dv_z}{dt} = \frac{d^2z}{dt^2} = -\frac{e}{m}\left[-B_{ext,r}(\vec{r})\, v_\phi + B_{RF}(\vec{r},t)\, v_r\right] \tag{3}$$

where $-e$ and m are the electron charge and electron mass at rest, respectively; $\vec{r}$ is the vector position, t is the time, (r, ϕ, z) are the cylindrical coordinates; ($v_r = \frac{dr}{dt}$, $v_\phi = r\,\frac{d\phi}{dt}$, $v_z = \frac{dz}{dt}$) are the corresponding components of the electron velocity; $\vec{E}_{sc} = E_{sc}\,\hat{r}$ is the electric field that takes into account the space charge effect; $\vec{E}_{RF} = E_{RF}\,\hat{r}$ and $\vec{B}_{RF} = B_{RF}\,\hat{\phi}$ are the electric and magnetic fields of the TEM coaxial mode; and $\vec{B}_{ext} = B_{ext,r}\,\hat{r} + B_{ext,z}\,\hat{z}$ is the external magnetic field.

B. Magnetic field produced by a hollow cylindrical magnet

In this subsection, we present the procedure to compute the magnetic field of an homogenously magnetized hollow cylinder in terms of the expressions of a simple homogenously magnetized cylinder. In Fig. 1 it is depicted the magnetized hollow cylinder under consideration, whose dimensions are b_1 and b_2 for the inner and outer radius of the cylinder, respectively; and h is the height. As indicated, the reference frame is centered in the mid-height of the cylinder.

First of all, we are going to present the magnetic field generated by a uniform cylinder with radius r_0. Static magnetic field of an homogenously magnetized cylinder can be derived using the equivalent volume and surface currents [18] determined as $\vec{J}_M = \nabla \times \vec{M}$ and $\vec{K}_M = \vec{M} \times \vec{n}$; $\vec{J}_M$ and $\vec{K}_M$ being the volume and the surface currents, respectively; $\vec{n}$ the unitary vector normal to the surface, and $\vec{M} = M\hat{z}$ the volume magnetization. Once the equivalent currents are obtained, the static magnetic field inside and outside the magnet can be calculated by means of the Ampere's Law [18], resulting the following expressions:

$$B_r(r,z) = \frac{\mu_0 M}{4\pi}\sqrt{\frac{16\,r_0}{r}}\left[\frac{E(k_2)}{k_2} - \frac{E(k_1)}{k_1} + \right.$$

$$\left. \frac{1}{k_1^2}\left(1 - \frac{k_1^2}{2}\right)K(k_1) - \left(1 - \frac{k_2^2}{2}\right)K(k_2)\right] \tag{4}$$

$$B_z(r,z) = \frac{\mu_0\, M}{2\pi\sqrt{r\,r_0}\left(1 + \frac{r}{r_0}\right)^2}\left[\left(z + \frac{h}{2}\right)\, k_2 \Pi\left(k_2, \sigma\right) + \right.$$

$$\left. - \left(z - \frac{h}{2}\right)\, k_1 \Pi\left(k_1, \sigma\right)\right] - \frac{r}{r_0} B_r(r,z) \tag{5}$$

$$\sigma \equiv \frac{4\,r\,r_0}{(r + r_0)^2}$$

$$k_1 \equiv \sqrt{\frac{4\,r\,r_0}{(r + r_0)^2 + \left(z - \frac{h}{2}\right)^2}}$$

$$k_2 \equiv \sqrt{\frac{4\,r\,r_0}{(r + r_0)^2 + \left(z + \frac{h}{2}\right)^2}}$$

where μ_0 is the magnetic permeability of vacuum; $K(k)$, $E(k)$ and $\Pi(k,\sigma)$ are the complete elliptic integrals of the first, the second and the third kind, respectively [19]. Note that the azimuthal magnetic field component is zero due to symmetry.

Finally, magnetic field expression for a hollow cylinder can be obtained by considering the superposition of the magnetic fields generated by two homogeneously magnetized cylinders with different radii, the same magnetization strength and opposite magnetization direction.

III. Simulation and experimental results

A. Uniform static axial magnetic field

The coaxial dimensions for multipactor simulations, as well as the testing sample, are as those employed in Ref. [8]. The experimental set-up is the standard one, commonly employed in multipactor measurements is shown in Fig. 2 (for a full-detailed description see [9]). The inner and outer radius dimensions are $a = 1.515$ mm and $b = 3.490$ mm, respectively; the gap length is $d = b - a = 1.975$ mm, the characteristic impedance is $Z_0 = 50\,\Omega$, and the length of the total sample is 90.4 mm. Both conductors were made of copper, with the following SEY parameters: first cross-over $W_1 = 25$ eV, the maximum SEY coefficient $\delta_{max} = 2.25$, and an incident electron energy for δ_{max} given by $W_{max} = 175$ eV. The uniform static axial magnetic field is applied by means of a long solenoid, where the sample in inserted.

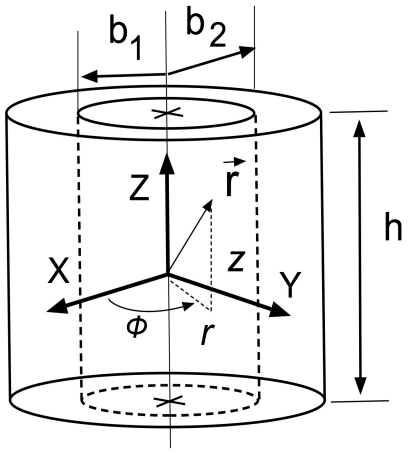

Fig. 1. The scheme of the hollow magnet with height h, and b_1 and b_2 radii.

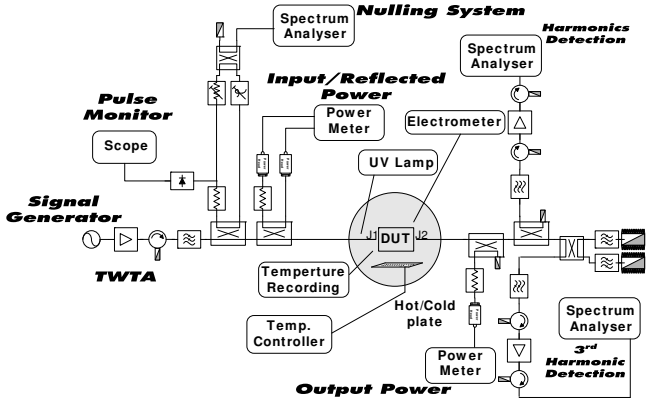

Fig. 2. Standard set-up used for multipactor measurements. In our experiment, three detection methods were employed: nulling system, third harmonic detection and electron probe. Pressure was in an interval 10^{-5}-10^{-7} mbar during the experiments. RF signal generator operated in pulsed mode with a pulse width of $20\,\mu$s and duty cycle of 2%.

Theoretical results show that multipactor resonant electron trajectories are disturbed by the presence of an external uniform axial DC magnetic field [8]. In this case, the equations of motion of the effective electron are simplified since $B_{ext,r} = 0$. The effect of such an axial magnetic field in the electron motion is the appearance of an azimuthal acceleration in eq. (2). This component of the acceleration bends the electron trajectories around the magnetic field flux lines, pushing the electron back to the departure conductor, allowing the presence of single-surface multipactor modes. Thus, the external magnetic field influences the electron flight time between successive impacts with the coaxial walls. In the numerical simulations, it has been found that the ratio between the cyclotron frequency $f_c = (eB_{DC})/(2\pi\, m)$, and the frequency of the RF electromagnetic field, plays a crucial role in the multipactor behavior, as reported in [4]. Fig. 3 reproduces this effect, where the multipactor RF power thresholds against the ratio of the cyclotron frequency to the microwave frequency are represented. Theoretical results predict that no multipactor discharge occurs when the ratio f_c/f exceeds a certain limit that varies depending on the

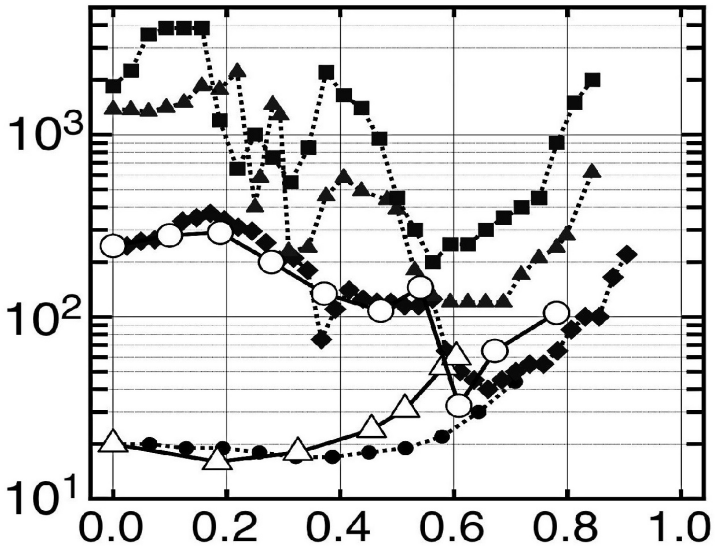

Fig. 3. Comparison of the experimental multipactor power threshold levels in Watts (solid lines) with the numerical simulations (dashed lines) against the ratio f_c/f. Numerical simulations: $f = 0.435$ GHz, solid circle; $f = 1.145$ GHz, solid diamond; $f = 2.000$ GHz, solid triangle; $f = 3.000$ GHz, solid square. Experimental data: $f = 0.435$ GHz, open triangle; $f = 1.145$ GHz, open circle. It is covered the f_c/f range where multipactor is expected to trigger.

RF signal frequency. For the investigated range the numerical calculations show that this critical quotient is within the range $f_c/f \in [0.7, 1]$. It should be remarked that the analyzed RF frequency range is wide enough to cover the most suitable frequency gap zone for the multipactor discharge.

Multipactor mitigation phenomenon can be understood in terms of the electron resonant trajectories. The classical theory of multipactor states that the time between two successive impacts must be an odd (even) number of RF semiperiods for double (single) surface multipactor modes. In numerical simulations it has been found that the electron flight time between successive impacts decreases as the ratio f_c/f increases. If the flight time is too short, the electron will never be able to synchronize with the RF electric field and, consequently, the electron kinetic energy at the impacts will be too low to release secondaries. In Ref. [8] the case of $f = 1.145$ GHz in Fig. 3 was analyzed by examining the electron trajectories at some relevant points of the multipactor power threshold curve. It was found that as the external axial magnetic field increases for a fixed RF frequency (i.e. the ratio f_c/f grows), the multipactor order diminishes. Moreover, the applied magnetic field introduces single-sided multipactor modes. According to classical resonance modes, the lower multipactor single-surface order possible is two. If the ratio f_c/f is such that the flight time of the electron is below two RF semiperiods, the resonance between the electron and the RF electric field cannot be achieved, and consequently, no multipactor discharge is possible.

Experimental measurements were performed at RF frequencies of $f = 1.145$ GHz and $f = 0.435$ GHz in order to validate the previous theoretical simulations. These results are shown in Fig. 3 together with the theoretical ones. It should

TABLE I
MEASURED POINTS FOR $f = 1.145$ GHZ WHERE NO MULTIPACTOR DISCHARGE WAS FOUND UP TO P_{max}

B_{DC} (mT)	f_c/f	P_{max} (W)
34.25	0.837	1450
37.56	0.918	1450
68.43	1.673	1450

TABLE II
MEASURED POINTS FOR $f = 0.435$ GHZ WHERE NO MULTIPACTOR DISCHARGE WAS FOUND UP TO P_{max}

B_{DC} (mT)	f_c/f	P_{max} (W)
10.0	0.644	120
11.5	0.710	120
13.3	0.856	120
14.8	0.952	120
15.2	0.978	120
18.9	1.216	120

be mentioned that although some experimental measurements for $f = 1.145$ GHz were previously presented in [8], new measurements have been performed in order to explore the multipactor-free zone for higher f_c/f values. These new measurements are summarized in Table I, where it is indicated the magnitude of the static axial magnetic field B_{DC}, the corresponding ratio f_c/f, and the maximum level of RF input power available in the experimental test-bed P_{max}. No multipactor discharge was found up to P_{max}, as well as in Table II for $f = 0.435$ GHz. Two additional checks were performed at $f = 0.435$ GHz in order to confirm that large f_c/f ratios hinder the multipactor breakdown. First, the RF input power was fixed at 60 W and the axial magnetic field was ranged from 8.9 mT ($f_c/f = 0.572$) to 19.0 mT ($f_c/f = 1.223$). Secondly, the RF input power was fixed at 120 W and the axial magnetic field was swept from 15.1 mT ($f_c/f = 0.972$) to 57.0 mT ($f_c/f = 3.668$). No multipactor discharge was observed in any of the two aforementioned tests.

Our experimental data and numerical calculations are in good agreement and suggest that electron multiplication is precluded over a f_c/f threshold. This fact proves the multipactor discharge suppression by a uniform DC magnetic field along the waveguide axis. However small discrepancies exist between the theoretical values and the experimental f_c/f thresholds that delimit the multipactor free domain. These small discrepancies between the experimental data and numerical simulations would be basically caused by the inaccuracy of the SEY model as well as the assumed velocity distribution for the secondary electrons.

B. Non-uniform magnetic field

The results discussed in previous section evidence that a strong enough magnetic filed prevents the multipactor multiplication in coaxial lines. However, the experimental implementation which requires of heavy coils and power supplies is unpractical in most cases [8]. Alternatively, the multipactor breakdown might be attenuated or mitigated using the inhomogeneous magnetic field produced by a set of permanent magnets. In order to explore this possibility, the coaxial sample was introduced into a hollow cylindrical neodymium permanent magnet. Its magnetization and dimensions were determined to hinder the multipactor multiplication within the required microwave frequency range.

In our case the inner and outer coaxial radius are $a = 1.238$ mm and $b = 2.850$ mm, respectively; the gap between conductors is $d = b - a = 1.612$ mm, the characteristic impedance is $Z_0 = 50\,\Omega$, and the sample length is 41.0 mm. Both conductors were made of copper, with the following SEY parameters: $W_1 = 19.5$ eV, $\delta_{max} = 2.61$, and $W_{max} = 219.7$ eV.

The inner radius was selected to hold inside the coaxial sample leaving an small gap to allow the outgassing of the system. Later, a parametrical study was performed to study the effect of the variation of the outer radius in the magnetic field structure. The main effect of increasing the cylinder thickness (for a fixed magnetization value) is to enlarge the strength of the magnetic field inside the gap of the magnet. In our case, a thickness in the range from 2 to 4 mm is desirable (the minimum thickness is 2 mm due to manufacturing considerations). Therefore, the inner and outer radii for our prototype were $b_1 = 12.5$ mm and $b_2 = 16.5$ mm. In Fig. 4 it is represented the axial and radial magnetic field components of a hollow cylindrical magnet, as a function of the axial coordinate normalized to the magnet height, using the expressions derived in Section II-B. It is seen that the axial (radial) magnetic field component is symmetrical (anti-symmetrical) with respect to the plane $z = 0$. Moreover, it is also noticed that the axial magnetic field presents a local minimum (in absolute value) in the center of the magnet. When we move towards the magnet edge there is a local maximum and then the strength drops to zero. As shown in subsection III-A the higher the axial component B_z is the better multipactor suppression is achieved. As a consequence, it is desirable that the axial magnetic field over the coaxial sample is as high as possible. It is evident that a long magnet would provide a very high homogeneous central magnetic field region, but in practical implementation this prototype might disturb other microwave components and electronic circuits surrounding the coaxial sample. Thus, we have preferred to design a permanent magnet with the minimum height. To achieve that, the coaxial waveguide center must be axially aligned with the magnet geometrical center, since the highest axial magnetic field is reached approximately in the region described by $z/h \in [-0.3, 0.3]$, and it becomes weaker as we approach to the magnet edges. In order to avoid these low axial magnetic field zones, the magnet height is selected to be $5 - 10\%$ higher than the coaxial length. Finally, the height of the magnet has been chosen to be: $h = 44$ mm.

In Fig. 5 the multipactor RF input power threshold as a function of the frequency gap (gap remains fixed) is plotted for two configurations of the coaxial waveguide just described in this subsection. The first configuration corresponds to the coaxial line without the magnet; the second case is for the coaxial waveguide immersed in the neodymium magnet. These numerical calculations evidence the multipactor mitigation within a certain frequency gap range using the permanent magnet. The magnet inhibites the discharge below $f \times d = 4.030$ GHzmm ($f = 2.5$ GHz), which corresponds to $f_c/f = 1.12$ (f_c has been calculated in $z = 0$, $r = (b-a)/2$, the coaxial gap

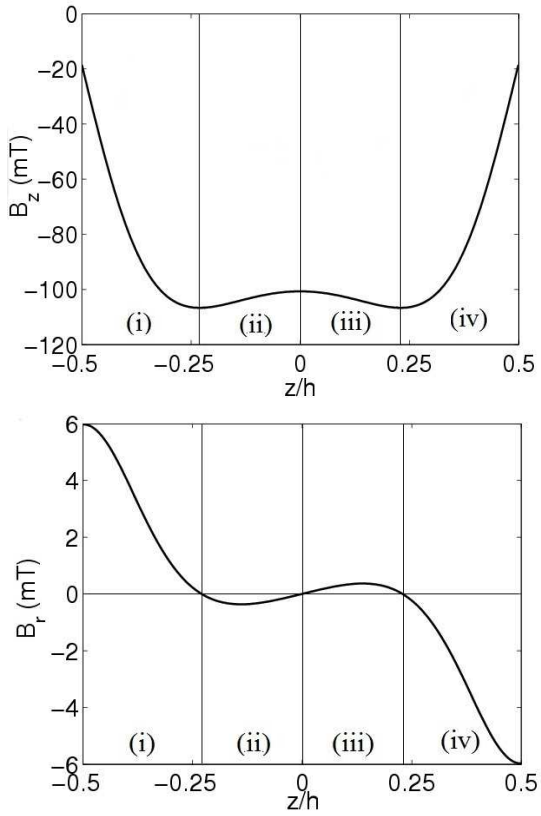

Fig. 4. The axial B_z and radial B_r components of Fig. 1 given by Eqs. 5 and 4 as a function of the normalized coordinate z/h. The value of the radial cylindrical coordinate has been chosen in the center of the coaxial gap, $r = 2.044$ mm. Magnet dimensions and properties: $b_1 = 12.5$ mm, $b_2 = 16.5$ mm, $h = 44$ mm, and $M = 1.153 \times 10^6$ A/m.

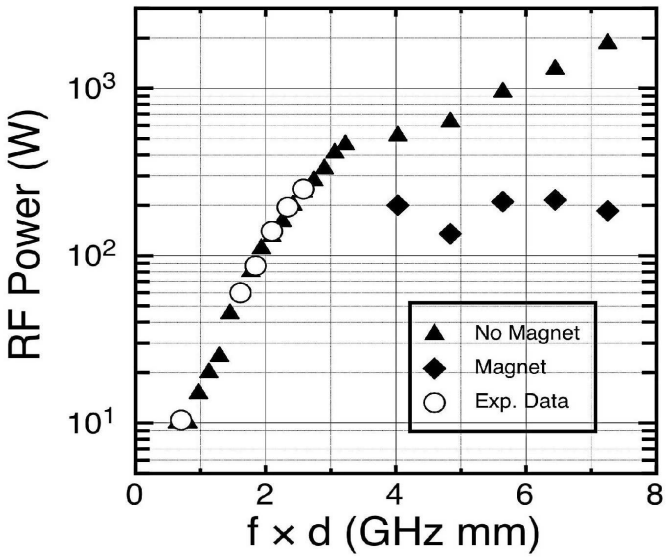

Fig. 5. Comparison of numerical calculations (solid symbols) with the experimental data (open symbols) without external magnetic field. The RF power thresholds are represented against the frequency gap (gap remains fixed). Note that multipactor discharge was not experimentally detected in the presence of the permanent magnet in the explored frequency range.

point where the axial magnetic field is maximum). It should be mentioned that multipactor appears above such frequency gap value with an RF power threshold lower than for the case without magnet. This fact is due to the appearance of single-surface multipactor mode, that may have a multipactor threshold even lower than the classical double-surface multipactor resonance [8], [20].

Despite the non-uniform magnetic field, the multipactor threshold for a coaxial waveguide immersed in a hollow cylindrical magnet, is similar to those of subsection III-A. Next, we analyze the electron trapping in the waveguide under the inhomogeneous magnetic field. First, from Fig. 4 the radial component $B_r \ll B_z$ and therefore the axial magnetic field strength B_z is dominant for the electron motion. This fact allows to neglect the term $B_{ext,r}\, v_z$ with respect to $B_{ext,z}\, v_r$ in (2). Additionally, for the considered RF power range the microwave magnetic field B_{RF} is also negligible compared with B_z. Thus, the terms $v\, B_{RF}$ could be dropped from Eqs. 1 and 3. Typical values of the aforementioned terms obtained in the numerical simulations are $B_{ext,r}\, v \sim 10^4$ T m/s, $B_{ext,z}\, v \sim 10^5$ T m/s and $v\, B_{RF} \sim 10^3$ T m/s. Eqs. 1, 2 and 3 for the earlier stages of the electron multiplication become,

$$\frac{dv_r}{dt} \approx -\frac{e}{m}\left[E_{RF}(\vec{r},t) + B_{ext,z}(\vec{r})\, v_\phi\right] \tag{6}$$

$$\frac{dv_\phi}{dt} \approx \frac{e}{m} B_{ext,z}(\vec{r})\, v_r \tag{7}$$

$$\frac{dv_z}{dt} \approx \frac{e}{m} B_{ext,r}(\vec{r})\, v_\phi \tag{8}$$

For this electron trapping argumentation we do not consider the electron acceleration caused by the microwave electric field. For this situation [21], the electron trajectories are found to spin around magnetic field lines with an angular frequency of $\vec{\omega}_c = (e/m)\vec{B}$. If the axial magnetic field is oriented along the $-z$ direction, the electron will spin clockwise leading to $v_\phi < 0$ since $v_\phi = r\,(d\phi/dt)$ (and $d\phi/dt < 0$ for clockwise rotation). Despite the presence of the RF electric field in our case, we can assume that the electron will still spin with $v_\phi < 0$. As a consequence, the axial acceleration approximated by (8) will be positive or negative depending only on the value of B_r. If $B_r > 0$, then $B_r\, v_\phi < 0$ and $dv_z/dt < 0$. Otherwise, if $B_r < 0$, then $B_r\, v_\phi > 0$ and $dv_z/dt > 0$. As it can be noticed from observing Fig. 4, the radial magnetic field has zeros at the points $z = -z_c$, $z = 0$, and $z = z_c$. According to this, we can delimit four regions for the axial electron cynematics as follows:

(i) $z < -z_c$, $B_r > 0$, $(dv_z/dt) < 0$
(ii) $-z_c < z < 0$, $B_r < 0$, $(dv_z/dt) > 0$
(iii) $0 < z < z_c$, $B_r > 0$, $(dv_z/dt) < 0$
(iv) $z > z_c$, $B_r < 0$, $(dv_z/dt) > 0$

Thus, an electron starting from zone (i) will be pushed towards $-z$, and will eventually leave the coaxial waveguide inhibiting the multipactor discharge. However, if the electron is initially in the region (ii), it will be pushed towards $+z$, and may

reach the region (iii). Now, in the zone (iii), the electron will be accelerated towards $-z$, back to zone (ii). It is clear that an electron starting from zone (ii) will tend to move between zones (ii) and (iii) indefinitely, and therefore it will remain inside the coaxial line. Similar argumentation applies for an electron starting in region (iii). Finally, an electron initially placed in zone (iv) will be pushed towards $+z$ and will eventually leave the coaxial waveguide. In these conditions, only electrons starting from regions (ii) and (iii) will contribute to the multipactor discharge. This point is crucial since, if no radial magnetic field were present, multipactor would appear in regions (i) and (iv) at lower RF frequency than in the regions (ii) and (iii) (this is because the axial magnetic field is weaker in zones (i) and (iv) than in regions (ii) and (iii)), and thus the multipactor mitigation efficiency would be reduced. This fact is explained in accordance to the analysis of the uniform magnetic field of Subsection III-A. The multipactor mitigation takes place when the empirical condition $f_c/f > [0.7, 1]$ is roughly fulfilled. If we take the worst case in the previous condition we have that the multipactor should be mitigated for RF frequencies below f_c. In our case, the lowest axial magnetic field in regions (ii) and (iii) (in absolute value) is 100 mT (see Fig. 4), which gives a cyclotron frequency of $f_c = 2.8$ GHz ($f \times d = 4.5$ GHzmm). By inspecting Fig. 5, it is noticed that in fact no multipactor discharge is expected for RF frequencies below $f = 2.5$ GHz ($f \times d = 4.0$ GHzmm). However, in regions (i) and (iv) the axial magnetic fields are lower than in regions (ii) and (iii). Actually, the axial magnetic field in the borders of the coaxial waveguide is around 40 mT, which gives $f_c = 1.1$ GHz. Therefore, if the radial magnetic field were not present to expel the electron from the coaxial waveguide, multipactor would appear for RF frequencies above $f = 1.1$ GHz ($f \times d = 1.77$ GHzmm), which is not the case.

We assessed this analysis by inspecting typical electron trajectories calculated in numerical simulations of the multipactor breakdown. The microwave frequency was fixed within the multipactor mitigation range and electrons were launched from different axial initial positions. It was found that an electron released from the zone (i), it was pushed out of the coaxial waveguide in few RF periods. It is also noticed that the growth rate in time of the electron population in the simulations is low enough to prevent the multipactor breakdown. On the other hand, if an electron starts its movement near the axis center, it remains within the central region, as discussed before. Although the electron does not leave the waveguide, the cumulative population quickly diminishes, so no multipactor discharge occurs.

Finally, the numerical simulations of Fig. 5 were assessed against a set of experimental tests. Coaxial and magnet properties are the same as described above in this Subsection. The experimental set-up for multipactor measurements is similar to the described in Subsection III-A. The multipactor breakdown was detected without the permanent magnet within the P-band test at $f = 0.435$ GHz ($f \times d = 0.701$ GHzmm). These results are represented in Fig. 5 and are in agreement with the theoretical predictions. On the contrary, no electron multiplication was detected when the coaxial sample was placed inside the hollow magnet up to the maximum RF power available of 100 W. The second test series were carried out within the L-band for the frequencies: $f = 1.0$ GHz ($f \times d = 1.612$ GHzmm), $f = 1.145$ GHz ($f \times d = 1.845$ GHzmm), $f = 1.3$ GHz ($f \times d = 2.096$ GHzmm), $f = 1.45$ GHz ($f \times d = 2.337$ GHzmm) and $f = 1.6$ GHz ($f \times d = 2.579$ GHzmm). Again, the multipactor discharges trigger for RF power levels in agreement with the theoretical simulations as evidence the results of Fig. 5. When the magnet is present, no multipactor breakdown appeared (in this case the maximum available RF input power was 360 W), in good concordance with the theory. Despite that theoretical simulations explore frequency values up to 4.96 GHz (8 GHzmm, see Fig. 5), the return losses of the coaxial sample increases at RF frequencies above the L-band. If the return loss increases we will have a considerable fraction of the input RF power being reflected by the coaxial sample, and as a consequence the RF amplifier might be damaged during the multipactor test. In order to avoid this, the frequency range of the multipactor measurements presented is restricted to P-band and L-band, both in the magnet and without magnet configurations.

IV. Conclusions

In this paper, we have studied the possible mitigation of the multipactor discharge in coaxial waveguides by means of an external magnetic field. First, we have analyzed the most simple scenario of a coaxial line immersed into an axial static magnetic field. The numerical simulations evidence that no multipactor discharge triggers when a strong enough external magnetic field is applied. Our experimental results are in good agreement with the theoretical calculations. Next, we have analyzed the case of a coaxial line immersed in a hollow cylindrical magnet. The multipactor simulations predicted the suppression of the discharge for RF frequencies below a certain value which depends on the specific magnetic field properties. Finally, a strong magnetized neodymium magnet was designed and manufactured. A multipactor test campaing was performed in order to validate the theoretical results. The experimental measurements in P-band and L-band are in good agreement with the simulations, demonstrating the capability of permanent magnets for multipactor suppression.

Acknowledgment

Our acknowledgement to the European High Power RF Space Laboratory and to the European High Power Space Materials Laboratory of Val Space Consortium for their contribution - Laboratories co-funded by the European Regional Development Fund - A way of making Europe.

References

[1] J. Vaughan, "Multipactor", *IEEE Trans. Electron Devices*, Vol. 35, No. 7, pp. 1172-1180, July 1988.

[2] G. Becerra "Studies of Coaxial Multipactor in Presence of a Magnetic Field", PSFC/RR-07-6, DOE/ET-54512-359, M.I.T., May 2007.

[3] R.L. Geng, H. Padamsee, S. Belomestnykh, P. Goudket, D.M. Dykes, R.G. Carter, "Suppression of multipacting in rectangular coupler waveguides", *Nuclear Instrum. Methods Physics Res. A*, Vol. 508, pp. 227-238, 2003.

[4] V. E. Semenov, N. A. Zharova, N. I. Zaitsev, A. K. Gvozdev, A. A. Sorokin, M. Lisak, J. Rasch, J. Puech, "Reduction of the Multipactor Threshold Due to Electron Cyclotron Resonance", *IEEE Transactions on Plasma Science*, vol. 40, no. 11, pp.3062-3069, Nov. 2012.

[5] S. Riyopoulos, D. Chernin, D. Dialetis, "Theory of multipactor in crossed fields", *Physics of Plasmas*, vol. 2, no. 8, pp. 3194-3212, Aug. 1995.

[6] E.C.A. Akoma Henry, D. A. Ogundele, O. Agboola, Y. A. Adediran, "Matlab analysis of the DC magnetic fields multipactor suppression model for rectangular waveguides", *3rd International Conference on Advanced Computer Theory and Engineering (ICACTE)*, vol.4, pp.97-101, 20-22 Aug. 2010.

[7] Akoma Henry, Acediran Y., "Suppression of Multipactor Breakdown in Satellite Rectangular Waveguides using DC Magnetic Fields", *Comput. Automation Engin. Conf. (ICCAE) 2010*, Vol. 1, pp. 766-770, Febr. 2010.

[8] D. González-Iglesias, A. M. Pérez, S. Anza, J. Vague, B. Gimeno, V.E. Boria, D. Raboso, C. Vicente, J. Gil, F. Caspers, and L. Conde "Multipactor in a Coaxial Line Under the Presence of an Axial DC Magnetic Field", *IEEE Electron Device Letters*, Vol. 33, no. 5, May 2012.

[9] "Multipaction design and test", ECSS-E-20-01A, ESA-ESTEC, 2003

[10] E. Somersalo, P. Yl-Oijala, D. Proch, and J. Sarvas, "Computational methods for analyzing electron multipacting in RF structures", *Part. Accel.*, vol. 59, pp. 107-141, 19980.

[11] A. M. Pérez, C. Tienda, C. Vicente, S. Anza, J. Gil, B. Gimeno, V. E. Boria, "Prediction of Multipactor Breakdown Thresholds in Coaxial Transmission Lines for Traveling, Standing, and Mixed Waves", *IEEE Trans. Plasma Science*, Vol. 37, no. 10, Oct. 2009.

[12] L. Verlet, "Computer 'experiments' on classical fluids. I. Thermodynamical properties of Lennard-Jones molecules", *Phys. Rev.*, vol. 159, no. 1, pp. 98-103, Jul. 1967

[13] C. Vicente, M. Mattes, D. Wolk, B. Mottet, H.L. Hartnagel, J.R. Mosig and D. Raboso, "Multipactor breakdown prediction in rectangular waveguide based components", *Microwave Symposium Digest, 2005 IEEE MTT-S International*, 12-17 June 2005.

[14] J.R.M. Vaughan, "Secondary Emission Formulas", *IEEE Trans. Electron Devices*, Vol. 40, no. 4, pp. 830, April 1993.

[15] J. Greenwood, "The correct and incorrect generation of a cosine distribution of scattered particles for Monte-Carlo modelling of vacuum systems", *Vacuum* vol. 67, no. 2, pp. 217-222, September 2002.

[16] T. P. Graves, "Experimental investigation of electron multipactor discharges at very high frequency", Ph.D. dissertation, *MIT Press* Cambridge, MA, 2006.

[17] J. W. Gewartowski and H. A. Watson, *Principles of electron tubes.* D. Van Nostrand Company, INC, Princeton, NJ, 1965.

[18] D. J. Griffiths, *Introduction to Electrodynamics.* Third Edition, Pearson Benjamin Cummings, 2008.

[19] M. Abramowitz, I. Stegund, *Handbook of Mathematical Functions with Formulas, Graphs, and Mathematical Tables*. Dover Publications ISBN 978-0-486-61272-0

[20] D. González-Iglesias, B. Gimeno. V. E. Boria, Á. Gómez, A. Vegas "Multipactor Effect in a Parallel-Plate Waveguide Partially Filled With Magnetized Ferrite", *Accepted for publication in IEEE Transactions on Electron Devices*,

[21] R. K. Wangsness, *Electromagnetic Fields.* Ed. Wiley, 2th edition, 1986.